

# GELATO: Geometrically Enriched Latent Model for Offline Reinforcement Learning

Guy Tennenholtz<sup>1</sup> Nir Baram<sup>1</sup> Shie Mannor<sup>1</sup>

## Abstract

Offline reinforcement learning approaches can generally be divided to proximal and uncertainty-aware methods. In this work, we demonstrate the benefit of combining the two in a latent variational model. We impose a latent representation of states and actions and leverage its intrinsic Riemannian geometry to measure distance of latent samples to the data. Our proposed metrics measure both the quality of out of distribution samples as well as the discrepancy of examples in the data. We integrate our metrics in a model-based offline optimization framework, in which proximity and uncertainty can be carefully controlled. We illustrate the geodesics on a simple grid-like environment, depicting its natural inherent topology. Finally, we analyze our approach and improve upon contemporary offline RL benchmarks.

## 1. Introduction

Offline reinforcement learning (offline RL) (Levine et al., 2020), a.k.a. batch-mode reinforcement learning (Ernst et al., 2005; Riedmiller, 2005; Fonteneau et al., 2013), involves learning a policy from potentially suboptimal data. In contrast to imitation learning (Schaal, 1999), offline RL does not rely on expert demonstrations, but rather seeks to surpass the average performance of the agents that generated the data. Methodologies such as the gathering of new experience fall short in offline settings, requiring reassessment of fundamental learning paradigms (Buckman et al., 2020; Wang et al., 2020; Zanette, 2020).

Approaches for offline RL are generally categorized into proximal and uncertainty-aware methods. Methods based on proximity maintain similarity to the data distribution, constraining the policy to remain close to the behavior in the data (Laroche et al., 2019; Kumar et al., 2019; Fujimoto et al., 2019; Chen et al., 2020b; Swazinna et al., 2020; Ku-

mar et al., 2020). In contrast, uncertainty-aware methods rely on bounding the validity of out of distribution (OOD) estimations. Such methods rely on conservative bounds over the “level of uncertainty” to control overestimation in OOD regions of the data (Kidambi et al., 2020; Yu et al., 2020; Buckman et al., 2020).

**How do we measure uncertainty?** Estimating uncertainty can be achieved via confidence sets (i.e., UCB and LCB) (Jaksch et al., 2010), ensemble methods (Osband et al., 2016; Yu et al., 2020), Monte-Carlo dropout (Gal & Ghahramani, 2016), or by modeling the distribution over functions (O’Donoghue et al., 2018). Nevertheless, estimating uncertainty from finite sequential data is a generally challenging task, depending on the coverage of the data (Nalisnick et al., 2018). Although proximal offline RL methods may be viewed as specialized instances of uncertainty-aware methods (Buckman et al., 2020), they benefit from robustness to errors in OOD regions where, in general, uncertainty measures may extrapolate poorly.

In this work we employ recent progress on the geometry of variational latent models (Arvanitidis et al., 2018; Kalatzis et al., 2020; Chen et al., 2020a; Arvanitidis et al., 2020) to control and mitigate the proximity-uncertainty tradeoff. Our offline RL framework penalizes an offline agent with accordance to a latent distance metric. As such, a central focus of this paper is on the construction of such a metric. Indeed, we construct a variational latent model which imposes a Riemannian submanifold in latent space. The induced metric, for which we derive analytical expression for in Section 5, can be represented as a union of two metrics; namely, a metric of proximity and a metric of uncertainty. We depict the geodesics of the induced metric on a grid-like environment, suggesting our latent model captures valuable structural dependencies. Finally we demonstrate the effectiveness of our metric on various continuous control benchmarks, showing improved performance over contemporary model-based offline RL approaches (Section 6).

Our contributions are as follows: (1) we introduce Riemannian geometry of generative models to reinforcement learning, (2) we offer a novel measure of out-of-distribution detection for RL, taking into account both proximity and uncertainty, and (3) our metric improves upon current ap-

<sup>1</sup>Technion, Israel Institute of Technology. Correspondence to: Guy Tennenholtz <guytenn@gmail.com>.

proaches in offline RL demonstrating robustness and adaptability. Finally, we discuss limitation as well as future applications of our approach w.r.t. our proposed metric.

## 2. Preliminaries

### 2.1. Offline Reinforcement Learning

We consider the standard Markov Decision Process (MDP) framework (Sutton et al., 1998) defined by the tuple  $(\mathcal{S}, \mathcal{A}, r, P, \alpha)$ , where  $\mathcal{S}$  is the state space,  $\mathcal{A}$  the action space,  $r : \mathcal{S} \times \mathcal{A} \mapsto [0, 1]$  the reward function,  $P : \mathcal{S} \times \mathcal{A} \times \mathcal{S} \mapsto [0, 1]$  the transition kernel, and  $\alpha \in (0, 1)$  is the discount factor.

In the online setting of reinforcement learning (RL), the environment initiates at some state  $s_0 \sim \rho_0$ . At any time step the environment is in a state  $s \in \mathcal{S}$ , an agent takes an action  $a \in \mathcal{A}$  and receives a reward  $r(s, a)$  from the environment as a result of this action. The environment transitions to state  $s'$  according to the transition function  $P(\cdot|s, a)$ . The goal of online RL is to find a policy  $\pi(a|s)$  that maximizes the expected discounted return  $v^\pi = \mathbb{E}_\pi \left[ \sum_{t=0}^{\infty} \alpha^t r(s_t, a_t) | s_0 \sim \rho_0 \right]$ .

Unlike the online setting, the offline setup considers a dataset  $\mathcal{D}_n = \{s_i, a_i, r_i, s'_i\}_{i=1}^n$  of transitions generated by some unknown agents. The objective of offline RL is to find the best policy in the test environment (i.e., real MDP) given only access to the data generated by the unknown agents.

**Model-based Offline Policy Optimization.** In this work we utilize a recently proposed model-based offline RL framework (MOPO, Yu et al. (2020)). Specifically, we assume access to an approximate MDP  $(\mathcal{S}, \mathcal{A}, \hat{r}, \hat{P}, \alpha)$ , and an admissible oracle uncertainty quantification module  $U : \mathcal{S} \times \mathcal{A} \mapsto \mathbb{R}$  which provides an upper bound on the error of the model, i.e.,

$$d(P(\cdot|s, a), \hat{P}(\cdot|s, a)) \leq U(s, a), \forall s \in \mathcal{S}, a \in \mathcal{A},$$

where  $d$  is some integral probability metric. MOPO defines an alternative reward-penalized MDP  $(\mathcal{S}, \mathcal{A}, \tilde{r}, \hat{P}, \alpha)$ , where

$$\tilde{r}(s, a) = \hat{r}(s, a) - \lambda U(s, a), \forall s \in \mathcal{S}, a \in \mathcal{A},$$

and solves the offline RL problem by executing an online algorithm in the reward-penalized (simulated) MDP.

### 2.2. Riemannian Manifolds

We define the Riemannian pullback metric, a fundamental component of our proposed method. We refer the reader to Carmo (1992) for further details on Riemannian geometry.

We are interested in studying a smooth surface  $M$  with a Riemannian metric  $g$ . A Riemannian metric is a smooth function that assigns a symmetric positive definite matrix

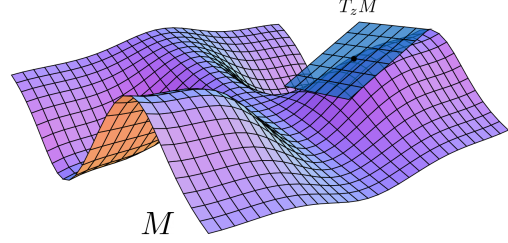


Figure 1. The tangent space of a Riemannian manifold at point  $z$ .

to any point in  $M$ . At each point  $z \in M$  a tangent space  $T_z M$  specifies the pointing direction of vectors “along” the surface (see Figure 1). The fact that  $M$  is smooth implies that the inner product of the metric space has local smooth changes throughout space, as formally defined below.

**Definition 1.** Let  $M$  be a smooth manifold. A Riemannian metric  $g$  on  $M$  changes smoothly and defines a real scalar product on the tangent space  $T_z M$  for any  $z \in M$  as

$$g_z(x, y) = \langle x, y \rangle_z = \langle x, G(z)y \rangle, \quad x, y \in T_z M,$$

where  $G(z) \in \mathbb{R}^{d_z \times d_z}$  is the corresponding metric tensor. The pair  $(M, g)$  is called a Riemannian manifold.

The Riemannian metric enables us to easily define geodesic curves. Consider some differentiable mapping  $\gamma : [0, 1] \mapsto M \subseteq \mathbb{R}^{d_z}$ , such that  $\gamma(0) = z_0, \gamma(1) = z_1$ . The length of the curve  $\gamma$  measured on  $M$  is given by

$$L(\gamma) = \int_0^1 \sqrt{\left\langle \frac{\partial \gamma(t)}{\partial t}, G(\gamma(t)) \frac{\partial \gamma(t)}{\partial t} \right\rangle} dt. \quad (1)$$

The geodesic distance  $d(z_1, z_2)$  between any two points  $z_1, z_2 \in M$  is then the infimum length over all curves  $\gamma$  for which  $\gamma(0) = z_0, \gamma(1) = z_1$ . That is,

$$d(z_1, z_2) = \inf_{\gamma} L(\gamma) \quad \text{s.t. } \gamma(0) = z_0, \gamma(1) = z_1.$$

The geodesic distance can be found by solving a system of nonlinear ordinary differential equations (ODEs) defined in the intrinsic coordinates (Carmo, 1992).

**Pullback Metric.** Assume an ambient (observation) space  $\mathcal{X}$  and its respective Riemannian manifold  $(M_{\mathcal{X}}, g_{\mathcal{X}})$ . Learning  $g_{\mathcal{X}}$  can be hard (e.g., learning the distance metric between images). Still, it may be captured through a low dimensional submanifold. As such, it is many times convenient to parameterize the surface  $M_{\mathcal{X}}$  by a latent space  $\mathcal{Z} = \mathbb{R}^{d_z}$  and a smooth function  $f : \mathcal{Z} \mapsto \mathcal{X}$ , where  $\mathcal{Z}$  is a low dimensional latent embedding space. As learning the metric of the manifold  $M_{\mathcal{X}}$  is hard or unknown, we turn to learning the immersed low dimensional submanifold  $M_{\mathcal{Z}}$  (for which the chart maps are trivial, since  $\mathcal{Z} = \mathbb{R}^{d_z}$ ).

---

**Algorithm 1** GELATO: Geometrically Enriched LATent model for Offline reinforcement learning
 

---

- 1: **Input:** Offline dataset  $\mathcal{D}$ , RL algorithm
  - 2: Train variational latent forward model on dataset  $\mathcal{D}$  by maximizing ELBO (Equation (5))
  - 3: Construct approximate MDP  $(\mathcal{Z}, \mathcal{A}, \hat{r}, \hat{P}, \alpha)$
  - 4: Define  $\tilde{r}_d(z, a) = \hat{r}(z, a) - \lambda \left( \frac{1}{K} \sum_{k=1}^K d(E_{z,a}, \text{NN}_{z,a}^{(k)}) \right)$ , with distance  $d$  induced by  $G_{D \circ F}$  (Proposition 2)
  - 5: Train RL algorithm over penalized MDP  $(\mathcal{Z}, \mathcal{A}, \tilde{r}_d, \hat{P}, \alpha)$
- 

Given a curve  $\gamma : [0, 1] \mapsto M_{\mathcal{Z}}$  we have that

$$\begin{aligned} & \left\langle \frac{\partial f(\gamma(t))}{\partial t}, G_{\mathcal{X}}(f(\gamma(t))) \frac{\partial f(\gamma(t))}{\partial t} \right\rangle \\ &= \left\langle \frac{\partial \gamma(t)}{\partial t}, J_f^T(\gamma(t)) G_{\mathcal{X}}(f(\gamma(t))) J_f(\gamma(t)) \frac{\partial \gamma(t)}{\partial t} \right\rangle, \end{aligned}$$

where the Jacobian matrix  $J_f(z) = \frac{\partial f}{\partial z} \in \mathbb{R}^{d_{\mathcal{X}} \times d_{\mathcal{Z}}}$  maps tangent vectors in  $TM_{\mathcal{Z}}$  to tangent vectors in  $TM_{\mathcal{X}}$ . The induced metric is thus given by  $G_{\mathcal{Z}}(z) = J_f(z)^T G_{\mathcal{X}}(f(z)) J_f(z)$ .

As  $G_{\mathcal{X}}$  is unknown, we approximate  $G_{\mathcal{Z}}$  by

$$G_{\mathcal{Z}}(z) = J_f(z)^T J_f(z). \quad (2)$$

The metric  $G_{\mathcal{Z}}$  is known as the *pullback metric*, as it ‘pulls back’ the metric  $G_{\mathcal{X}}$  on  $\mathcal{X}$  back to  $G_{\mathcal{Z}}$  via  $f : \mathcal{Z} \mapsto \mathcal{X}$ . The pullback metric captures the intrinsic geometry of the immersed submanifold while taking into account the ambient space  $\mathcal{X}$ . The geodesic distance in ambient space is captured by geodesics in the latent space  $\mathcal{Z}$ , reducing the problem to learning the latent embedding space  $\mathcal{Z}$  and the observation function  $f$ .

### 3. GELATO: Geometrically Enriched LATent model for Offline reinforcement learning

Following the setup of MOPO (see Section 2.1), we assume access to an approximate model of the environment. We are interested in defining an admissible oracle uncertainty quantification module which would correctly quantify an upper bound on the error of our model. This problem is closely related to the OOD identification problem (Lakshminarayanan et al., 2017; Ren et al., 2019). Our work considers measuring the model’s error via a distance metric w.r.t. the given offline data. In Sections 4 and 5 we will carefully establish such a metric, yet, for purpose of clarity, we first present its use in an offline RL framework.

We begin by setting the notation for the latent space over which we will define our metric. Let  $\mathcal{Z}, \mathcal{E}$  denote state and state-action latent spaces, respectively. We also denote by  $E_{z,a} \in \mathcal{E}$  the state-action embedding of  $(z, a) \in \mathcal{Z} \times \mathcal{A}$ . Given a dataset  $\mathcal{D}_n = \{(s_i, a_i, r_i, s'_i)\}_{i=1}^n$  and metric over latent codes  $d : \mathcal{E} \times \mathcal{E} \mapsto \mathbb{R}_+$ , we define the reward-penalized MDP  $(\mathcal{Z}, \mathcal{A}, \tilde{r}_d, \hat{P}, \alpha)$ , where  $\tilde{r}_d$  is the penalized

reward given by

$$\tilde{r}_d(z, a) = \hat{r}(z, a) - \lambda \left( \frac{1}{K} \sum_{k=1}^K d(E_{z,a}, \text{NN}_{z,a}^{(k)}) \right). \quad (3)$$

Here,  $\text{NN}_{z,a}^{(k)}$  is the  $k^{\text{th}}$  nearest neighbor of  $E_{z,a}$  in  $\mathcal{D}$  w.r.t. the metric  $d$ . Note the sum over  $K$  nearest neighbors, allowing for more robust quantification of the distance.

Algorithm 1 presents our proposed approach. We begin by training a variational latent forward model (described in detail in Section 4), which maps states and actions to their respective latent spaces, next states, and rewards. Informally, our latent model induces a metric  $d$  over state-action embeddings (Section 5), where embeddings that are close w.r.t.  $d$  transition to similar states. Finally, having defined the penalized reward (Equation (3)), we train an RL algorithm over the penalized approximate MDP, i.e.,  $(\mathcal{Z}, \mathcal{A}, \tilde{r}_d, \hat{P}, \alpha)$ .

We are now ready to fill in the missing pieces of Algorithm 1. Specifically, in the next section we begin by defining our latent variable model – a building block of our proposed metric. Then, in Section 5 (the crux of our work), we will carefully construct a metric which captures both proximity and uncertainty w.r.t. the data, i.e., compute  $d$ . Finally in Section 6 we will demonstrate the effectiveness of our metric as implemented in Algorithm 1.

### 4. A Variational Latent Model

We begin by describing our variational forward model. The model, based on an encoder, latent forward function, and decoder framework assumes the underlying dynamics and reward are governed by a state-embedded latent space  $\mathcal{Z} \subseteq \mathbb{R}^{d_{\mathcal{Z}}}$ . The probability of a trajectory  $\tau = (s_0, a_0, r_0, \dots, s_h, a_h, r_h)$  is given by

$$\begin{aligned} P(\tau) &= \int_{z_0, \dots, z_h} P(z_0) \prod_{i=0}^h P(s_i | z_i) \pi(a_i | s_i) P(r_i | E_{z_i, a_i}) \\ &\quad \times \prod_{j=1}^h P(z_j | E_{z_{j-1}, a_{j-1}}) dz_0 \dots dz_h, \end{aligned} \quad (4)$$

where  $E : \mathcal{Z} \times \mathcal{A} \mapsto \mathcal{E} \subseteq \mathbb{R}^{d_{\mathcal{E}}}$  is a deterministic, invertible embedding function which maps pairs  $(z, a)$  to a state-action-embedded latent space  $\mathcal{E}$ .  $E_{z,a}$  is thus a sufficient

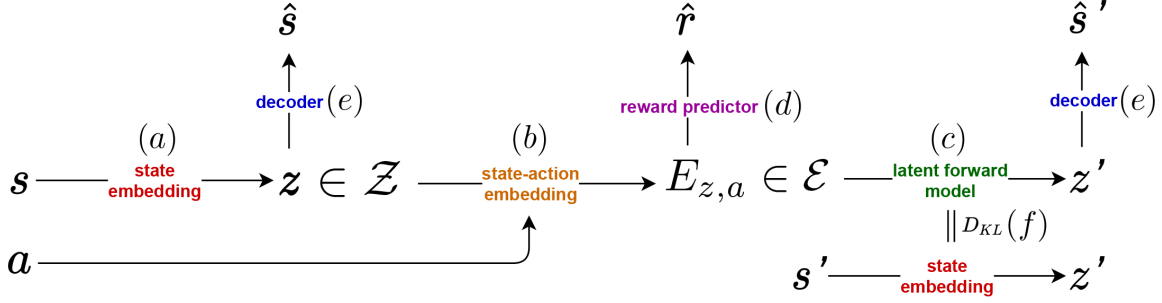


Figure 2. A graphical representation of our latent variable model. **(a)** The state  $s$  is embedded via the state embedding function (i.e., approximate posterior)  $z \sim q(\cdot|s)$ . **(b)** The action and embedded state pass through an invertible embedding function  $E$  to produce the state-action embedding  $E_{z,a}$ . **(c,d)** The state-action embedding is passed through a reward predictor and latent forward model,  $\hat{r} \sim P(\cdot|E_{z,a})$  and  $z' \sim P(\cdot|z, a)$ , respectively. **(e)** The next latent state  $z'$  is decoded back to observation space to generate  $\hat{s}' \sim P(\cdot|z')$ . **(f)** Finally, during training, the target state  $s'$  is embedded and compared to  $z'$  (by the KL-divergence term in Equation (5)), preserving the consistency of the latent space  $\mathcal{Z}$ .

statistic of  $(z, a)$ . The proposed graphical model is depicted in Figure 2. We note that an extension to the partially observable setting replaces  $s_t$  with  $h_t = (s_0, a_0, \dots, s_t)$ , a sufficient statistic of the unknown state.

Maximizing the log-likelihood  $\log P(\tau)$  is hard due to intractability of the integral in Equation (4). We therefore introduce the approximate posterior  $q(z|s)$  and maximize the evidence lower bound (see the appendix for derivation)

$$\begin{aligned} & \sum_{i=0}^h \mathbb{E}_{z_i \sim q(z_i|s_i)} \left[ \log(P(s_i | z_i) \pi(a_i | s_i) P(r_i | E_{z_i, a_i})) \right] \\ & - \sum_{i=0}^{h-1} \mathbb{E}_{z_i \sim q(z_i|s_i)} \left[ D_{KL}(q(z_{i+1} | s_{i+1}) || P(z_{i+1} | E_{z_i, a_i})) \right] \\ & - D_{KL}(q(z_0 | s_0) || P(z_0)). \end{aligned} \quad (5)$$

The distribution parameters of the approximate posterior  $q(z|s)$ , the likelihoods  $P(s|z)$ ,  $\pi(a|s)$ ,  $P(r|E_{z,a})$ , and the latent forward model  $P(z'|E_{z,a})$  are represented by neural networks. The invertible embedding function  $E$  is represented by an invertible neural network, e.g., affine coupling, commonly used for normalizing flows (Dinh et al., 2014). Though various latent distributions have been proposed (Klushyn et al., 2019; Kalatzis et al., 2020), we found Gaussian parametric distributions to suffice for all of our model’s functions. Particularly, we used two outputs for every distribution, representing the expectation  $\mu$  and variance  $\sigma$ . All networks were trained end-to-end to maximize the evidence lower bound in Equation (5).

Our latent variable model is designed to capture both the epistemic and aleatoric uncertainty (Senge et al., 2014). The variance output of the decoder captures epistemic uncertainty, while stochasticity of the latent forward model  $P(z'|E_{z,a})$  captures aleatoric uncertainty. For the purpose of offline RL, we will focus on the epistemic uncertainty of

our model.

We tested the quality of our variational model on datasets of two tasks in Minecraft (Guss et al., 2019); namely, a navigation task (150k examples) and a tree chopping task (250k examples), both generated by human players. The variational model was trained only on the navigation task. We embedded the data from both datasets using our trained model, and measured the decoder variance for all samples. Figure 3 depicts a TSNE projection of the latent space  $\mathcal{Z}$ , coloring in blue the navigation task and in red the tree chopping task. Light colors correspond to low variance (i.e., sharp images), whereas dark colors correspond to large variance (i.e. OOD samples). We found that our variational model was able to properly distinguish between the two tasks, with some overlap due to similarity in state space features. Additionally, we noticed a clear transition in decoding

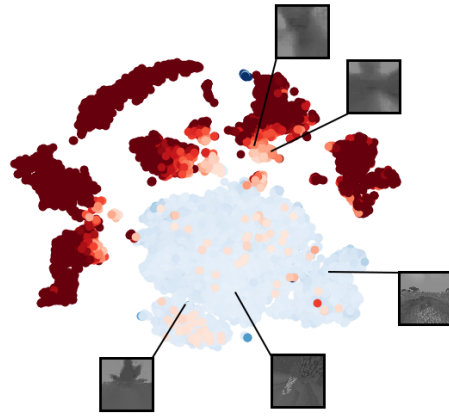


Figure 3. TSNE projection of latent space  $\mathcal{Z}$  for navigation dataset (blue) and tree chopping dataset (red) in Minecraft (Guss et al., 2019). Darker colors correspond to higher decoder variance.

variance as samples farther away from the trained latent data attained larger variance, suggesting our variational model was properly able to distinguish OOD samples.

We refer the reader to the appendix for further analysis and approaches of uncertainty quantification in variational models. In our experiments, we found that the standard decoder variance sufficed for all of the tested domains.

## 5. Metrics of Proximity and Uncertainty for Offline Reinforcement Learning

Having constructed our latent variable model we are now ready to define our proposed metric (i.e.,  $d(\cdot, \cdot)$  in Algorithm 1). Recall in Section 2.2, Equation (2), we defined the pullback metric w.r.t. some arbitrary smooth function  $f$  mapping latent variables to a known ambient (observation) space. In this section we specify candidates for  $f$  induced by our latent model, and relate them to metrics of proximity and uncertainty. Particularly, we derive analytical expressions for the decoder pullback metric, as well as composition of forward and decoder models. These pullback metrics, as we later show, capture intrinsic features of similarity w.r.t. the data as well as uncertainty estimates of OOD regions.

To this end, we are interested in learning a metric which adequately reflects the ‘‘similarity’’ between data points. Assuming we are able to accurately learn the latent spaces  $\mathcal{Z}, \mathcal{E}$ , we might favor using the Euclidean metric as a measure of distance. However, sharp discontinuities in latent codes may result in large deviations and significant errors (Chen et al., 2018). Instead, we treat  $\mathcal{Z}$  and  $\mathcal{E}$  as Riemannian manifolds. The geometry of these manifolds will be captured by the observation decoder function  $D(z) \sim P(s|z)$  and latent forward model  $F(E_{z,a}) \sim P(z'|E_{z,a})$ , as described next.

### COMBINING PROXIMITY AND UNCERTAINTY THROUGH LATENT GEODESICS

Recall the stochastic, differentiable functions given by our variational latent model. The (stochastic) latent forward model and decoder, which we denote by  $F : \mathcal{E} \mapsto \mathcal{Z}$  and  $D : \mathcal{Z} \mapsto \mathcal{S}$ , respectively, can be written as

$$\begin{aligned} F(\cdot) &= \mu_F(\cdot) + \sigma_F(\cdot) \odot \epsilon_F, \\ D(\cdot) &= \mu_D(\cdot) + \sigma_D(\cdot) \odot \epsilon_D, \end{aligned}$$

where  $\epsilon \sim \mathcal{N}(0, I)$ , and  $\mu, \sigma$  are the expectation and variance functions, respectively.

We begin by considering the pullback metric induced by  $f \in \{F, D\}$ . The following proposition is adopted from Arvanitidis et al. (2017). It gives an analytical expression for the expected pullback metric of  $f$ .

**Proposition 1.** *Let  $f \in \{F, D\}$  as defined above. Then, the expected pullback metric of  $f$  is given by*

$$\mathbb{E}[G_f] = \underbrace{J_{\mu_f}^T J_{\mu_f}}_{\text{proximity}} + \underbrace{J_{\sigma_f}^T J_{\sigma_f}}_{\text{uncertainty}}. \quad (6)$$

The expected metric in Equation (6) gives us a sense of the topology of the latent space manifold induced by  $f$ . The terms  $G_\mu = J_{\mu_f}^T J_{\mu_f}$  and  $G_\sigma = J_{\sigma_f}^T J_{\sigma_f}$  are in fact the induced pullback metrics of  $\mu$  and  $\sigma$ , respectively. As shortest geodesics will tend to follow small values of  $\|\mathbb{E}[G_f]\|$ ,  $G_\mu$  will keep away from areas with no latent codes, whereas  $G_\sigma$  will remain small in regions of low uncertainty. We therefore recognize  $G_\mu$  and  $G_\sigma$  as *metrics of proximity and uncertainty*, respectively.

Due to the inherent decoupling between proximity and uncertainty, it may be beneficial to control the curvature of the expected metric by only focusing on one of the metrics. Denoting  $\alpha_{\text{prox}} \in [0, 1]$  as the proximity coefficient, we define the skewed pullback metric of  $f$  as

$$G_f^\alpha = \alpha_{\text{prox}} G_\mu + (1 - \alpha_{\text{prox}}) G_\sigma. \quad (7)$$

The skewed pullback metric will become valueable in the following section, as we carefully control the tradeoff between proximity and uncertainty in the tested domains.

Next, we turn to analyze the pullback metric induced by our forward transition model. As both  $F$  and  $D$  are stochastic (capturing both epistemic and aleatoric uncertainty), the result of Proposition 1 cannot be directly applied to their composition. The following proposition provides an analytical expression for the expected pullback metric of  $D \circ F$ . Its proof can be found in the appendix.

**Proposition 2.** *Let  $F : \mathcal{E} \mapsto \mathcal{Z}$ , and  $D : \mathcal{Z} \mapsto \mathcal{S}$  as defined above. Then, the expected pullback metric of the composite function  $(D \circ F) : \mathcal{E} \mapsto \mathcal{S}$  is given by*

$$\mathbb{E}[G_{D \circ F}] = J_{\mu_F}^T \bar{G}_D J_{\mu_F} + J_{\sigma_F}^T \text{diag}(\bar{G}_D) J_{\sigma_F},$$

where here,  $\bar{G}_D = \mathbb{E}_{z' \sim F} [J_{\mu_D}^T J_{\mu_D} + J_{\sigma_D}^T J_{\sigma_D}]$  is the expected pullback metric of  $D$ .

Unlike the metric in Equation (6), the composite metric distorts the decoder metric with Jacobian matrices of the forward model statistics. The composite metric takes into account both proximity and uncertainty w.r.t. the ambient space as well as the latent forward model. As before, a skewed version of the metric can be designed, replacing  $\bar{G}_D$  with its skewed version.

The composite metric induces a measure of distance w.r.t. the Markov transition function. Particularly, a shortest geodesic curve between  $e_1, e_2 \in \mathcal{E}$  will obtain minimal energy in ambient space, i.e., minimize the integral of norm

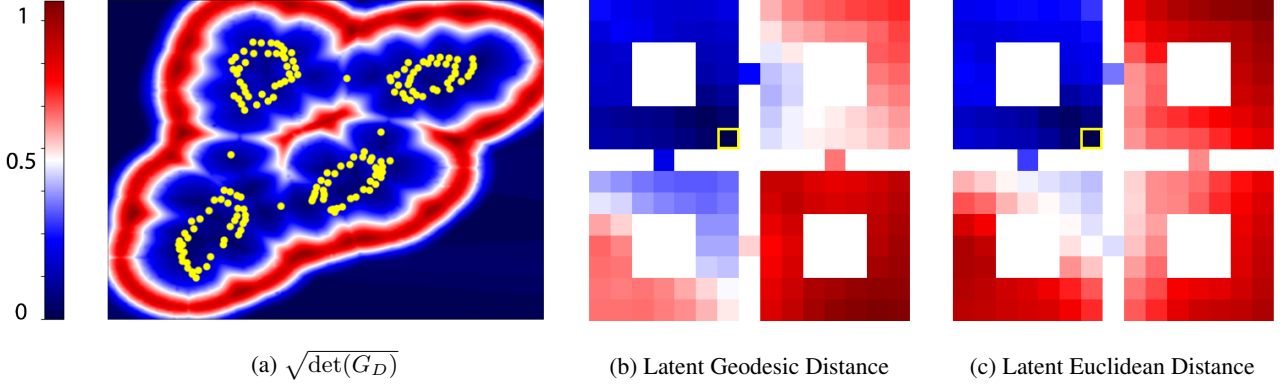


Figure 4. (a) The latent space (yellow markers) of the grid world environment and the geometric volume measure of the decoder-induced metric (background). (b, c) The geodesic distance of the decoder-induced submanifold and the Euclidean distance of latent states, as viewed in ambient space. All distances are calculated w.r.t. the yellow marked state. Note: colors in (a) are unrelated to colors in (b,c).

differences on a path between  $\hat{s}'_1$  and  $\hat{s}'_2$ . Alternatively, one could use the metric  $G_F$  instead to obtain shortest geodesics w.r.t.  $z'_1, z'_2$ . The choice of metric, though, depends on the domain at hand. In our experiments (Section 6) we found  $G_{D \circ F}$  to be a sufficient measure of distance for GELATO (Algorithm 1). See Section 8 for further discussion.

Having defined the needed distance metric for Algorithm 1, in the next section we illustrate its effectiveness in capturing the inherent geometry of the dynamic environment. We then demonstrate GELATO’s ability to improve offline RL performance on various continuous control benchmarks.

## 6. Experiments

In this section we will use the derived metrics of proximity and uncertainty in the context of offline RL. We begin by visualizing the proposed metric in a toy grid-world environment. We will then demonstrate the benefit of our approach in contemporary continuous control tasks.

### 6.1. Metric Visualization

To better understand the inherent structure of our metric, we constructed a grid-world environment for visualizing our proposed latent representation and metrics. The  $15 \times 15$  environment, as depicted in Figure 4, consists of four rooms, with impassable obstacles in their centers. The agent, residing at some position  $(x, y) \in [-1, 1]^2$  in the environment can take one of four actions: up, down, left, or right – moving the agent 1, 2 or 3 steps (uniformly distributed) in that direction. We collected a dataset of 10000 samples, taking random actions at random initializations of the environment. The ambient state space was represented by the position of the agent – a vector of dimension 2, normalized to values in  $[-1, 1]$ . Finally, our variational latent model was trained with latent dimension  $d_Z = 2$ .

The latent space output of our model is depicted by yellow markers in Figure 4a. Indeed, the latent embedding consists of four distinctive clusters, structured in a similar manner as our grid-world environment. Interestingly, the distortion of the latent space accurately depicts an intuitive notion of distance between states. As such, rooms are distinctively separated, with fair distance between each cluster. States of pathways between rooms clearly separate the room clusters, forming a topology with four discernible bottlenecks.

In addition to the latent embedding, Figure 4a depicts the geometric volume measure<sup>1</sup>  $\sqrt{\det(G_D)}$  of the trained pull-back metric induced by  $D$ . This quantity demonstrates the effective geodesic distances between states in the decoder-induced submanifold. Indeed geodesics between data points to points outside of the data manifold (i.e., outside of the red region), would attain high values as integrals over areas of high magnitude. In contrast, geodesics near the data manifold would attain low values.

Finally, we visualize the decoder-induced geodesic distance and compare it to the latent Euclidean distance in Figures 4b and 4c, respectively. The plots depict the normalized distances of all states to the state marked by a yellow square. Evidently, the geodesic distance captures a better notion of distance in the said environment, correctly exposing the “land distance” in ambient space. As expected, states residing in the bottom-right room are farthest from the source state, as reaching them comprises of passing through at least two bottleneck states. In contrast, the latent Euclidean distance does not properly capture these geodesics, exhibiting a similar distribution of distances in other rooms. Nevertheless, both geodesic and Euclidean distances reveal the intrinsic topological structure of the environment, that of which is not captured by the extrinsic

<sup>1</sup>The geometric volume measure captures the volume of an infinitesimal area in the latent space.

coordinates  $(x, y) \in [-1, 1]^2$ . Particularly, the state coordinates  $(x, y)$  would wrongly assign short distances to states across impassible walls or obstacles, i.e., measuring the “air distance”.

The grid-world environment demonstrates the inherent latent geometry of our variational model. In what follows, we will demonstrate the flexibility and robustness of the induced metrics on various offline RL tasks.

## 6.2. Continuous Control

We performed experiments to analyze GELATO on various continuous control datasets. Our experiments focused on the effect of proximity and uncertainty on overall performance.

**Datasets.** We used D4RL (Fu et al., 2020) as a benchmark for all of our experiments. We tested GELATO on three Mujoco (Todorov et al., 2012) environments (Hopper, Walker2d, Halfcheetah) on datasets generated by a single policy and a mixture of two policies. Specifically, we used datasets generated by a random agent (1M samples), a partially trained agent, i.e, medium agent (1M samples), and a mixture of partially trained and expert agents (2M samples).

**Implementation Details.** We trained our variational model with latent dimensions  $\dim(\mathcal{Z}) = 32$  and  $\dim(\mathcal{E}) = \dim(\mathcal{Z}) + \dim(\mathcal{A})$ . The latent model was trained for 100k steps by stochastic gradient descent with batch size of 256. We split training into two phases. First, the model was fully trained using a calibrated Gaussian decoder (Rybkin et al., 2020). Specifically, a maximum-likelihood estimate of the variance was used  $\sigma^* = \text{MSE}(\mu, \hat{\mu}) \in \arg \max_{\sigma} \mathcal{N}(\hat{\mu} | \mu, \sigma^2 I)$ . Then, in the second stage we fit the variance decoder network.

In order to practically estimate the geodesic distance in Algorithm 1, we defined a parametric curve in latent space and used gradient descent to minimize the curve’s energy. The resulting curve and pullback metric were then used to calculate the geodesic distance by a numerical estimate of the curve length (Equation (7)). An exhaustive overview of the estimation method can be found in the appendix.

We used FAISS (Johnson et al., 2019) for efficient GPU-based  $k$ -nearest neighbors calculation. In all our experiments we set  $K = 20$  neighbors for the penalized reward in Equation (3). Finally, we used a variant of Soft Learning, as proposed in Yu et al. (2020) as our RL algorithm, trained for 1M steps (see Appendix for further details).

**Proximity vs. Uncertainty.** To test GELATO we constructed two variants, trading off proximity and uncertainty through our latent-induced metric. Particularly, we denote by GELATO-UNC and GELATO-PROX variants which implement the skewed metric (see Equation (7)), with  $\alpha_{\text{prox}} = 0.1$  and  $\alpha_{\text{prox}} = 0.9$ , respectively. We compared

Hopper			
Method	Random	Medium	Med-Expert
DATA SCORE	299 ± 200	1021 ± 314	1849 ± 1560
<b>GELATO</b>	<b>685 ± 15</b>	<b>1676 ± 223</b>	<b>574 ± 16</b>
<b>GELATO-unc</b>	<b>481 ± 29</b>	<b>1158 ± 423</b>	<b>879 ± 153</b>
<b>GELATO-prox</b>	<b>240 ± 22</b>	<b>480 ± 15</b>	<b>920 ± 249</b>
MOPO	677 ± 13	1202 ± 400	1063 ± 193
MBPO	444 ± 193	457 ± 106	<b>2105 ± 1113</b>
SAC	664	325	1850
IMITATION	615	1234	3907
Walker2d			
Method	Random	Medium	Med-Expert
DATA SCORE	1 ± 6	498 ± 807	1062 ± 1576
<b>GELATO</b>	<b>412 ± 85</b>	<b>1269 ± 549</b>	<b>1515 ± 379</b>
<b>GELATO-unc</b>	<b>290 ± 79</b>	<b>487 ± 289</b>	<b>1473 ± 389</b>
<b>GELATO-prox</b>	<b>158 ± 35</b>	<b>571 ± 326</b>	<b>1596 ± 416</b>
MOPO	396 ± 76	518 ± 560	1296 ± 374
MBPO	251 ± 235	370 ± 221	222 ± 99
SAC	120	27	-2
IMITATION	47	193	329
Halfcheetah			
Method	Random	Medium	Med-Expert
DATA SCORE	-303 ± 79	3945 ± 494	8059 ± 4204
<b>GELATO</b>	<b>116 ± 43</b>	<b>5168 ± 849</b>	<b>6449 ± 2790</b>
<b>GELATO-unc</b>	<b>23 ± 35</b>	<b>3034 ± 585</b>	<b>7130 ± 3780</b>
<b>GELATO-prox</b>	<b>-28 ± 31</b>	<b>3300 ± 613</b>	<b>7412 ± 3166</b>
MOPO	<b>4114 ± 312</b>	4974 ± 200	7594 ± 4741
MBPO	3527 ± 487	3228 ± 2832	907 ± 1185
SAC	3502	-839	-78
IMITATION	-41	4201	4164

Table 1. Performance of GELATO and its variants in comparison to contemporary model-based methods on D4RL datasets. Scores correspond to the return ± standard deviation, averaged over 5 seeds. Results for MOPO, MBPO, SAC, and imitation are taken from Yu et al. (2020). Mean score of dataset added for reference. Highlighted scores show an exceptional score w.r.t other methods.

GELATO and its variants to contemporary model-based offline RL approaches; namely, MOPO (Yu et al., 2020) and MBPO (Janner et al., 2019), as well as the standard baselines of SAC (Haarnoja et al., 2018) and imitation (behavioral cloning).

Results for all of the tested domains are shown in Table 1. For the non-skewed version of GELATO we found significant performance increase on all medium datasets, i.e., partially trained agent. We believe this to be due to the inherent nature of our metric to take into account both proximity and uncertainty, allowing the agent to leverage proximity to the data in areas of high uncertainty. Since the medium dataset contained average behavior, mixing proximity benefited the agent’s overall performance.

In most of the tested datasets we found an increase in performance for at least one of the GELATO variants. The med-expert datasets showed better performance for the proximity-oriented metric. These suggest flexibility of our metric to increase performance when the quality of the dataset is known, a reasonable assumption in many domains. Moreover, the non-skewed version of GELATO, showed consistency over all datasets, favorably leveraging the strengths of proximity and uncertainty.

Finally, we noticed surprisingly bad performance in the random datasets. We conjecture this was due to errors in our latent model. These errors were compounded when integrated to compute the geodesic distance. More involved techniques of uncertainty estimation (e.g., ensemble of decoders) may reduce errors in our metrics (see Appendix for further discussion).

## 7. Related Work

**Offline Reinforcement Learning.** The field of offline RL has recently received much attention as several algorithmic approaches were able to surpass standard off-policy algorithms. Value-based online algorithms do not perform well under highly off-policy batch data (Fujimoto et al., 2019; Kumar et al., 2019; Fu et al., 2019; Fedus et al., 2020; Agarwal et al., 2020), much due to issues with bootstrapping from out-of-distribution (OOD) samples. These issues become more prominent in the offline setting, as new samples cannot be acquired.

Several works on offline RL have shown improved performance on standard continuous control benchmarks (Laroche et al., 2019; Kumar et al., 2019; Fujimoto et al., 2019; Chen et al., 2020b; Swazinna et al., 2020; Kidambi et al., 2020; Yu et al., 2020; Kumar et al., 2020). In this work we were specifically interested in model-based approaches (Yu et al., 2020; Kidambi et al., 2020), in which the agent is incentivized to remain close to areas of low uncertainty.

Our work focused on controlling uncertainty estimation in high dimensional environments. Our methodology utilized recent success on the geometry of deep generative models (Arvanitidis et al., 2018; 2020), proposing an alternative approach to uncertainty estimation. Finally, we considered a potential tradeoff between proximity and uncertainty, suggesting a benefit of leveraging both to improve performance.

**Representation Learning.** Representation learning seeks to find an appropriate representation of data for performing a machine-learning task (Goodfellow et al., 2016). Variational Auto Encoders (Kingma & Welling, 2013; Rezende et al., 2014) have been a popular representation learning technique, particularly in unsupervised learning regimes (Kingma et al., 2014; Sønderby et al., 2016; Chen et al., 2016; Van Den Oord et al., 2017; Hsu et al., 2017; Serban

et al., 2017; Engel et al., 2017; Bojanowski et al., 2018; Ding et al., 2020), though also in supervised learning and reinforcement learning (Hausman et al., 2018; Li et al., 2019; Petangoda et al., 2019; Hafner et al., 2019; 2020). Particularly, variational models have been shown able to derive successful behaviors in high dimensional benchmarks (Hafner et al., 2020).

Various representation techniques in reinforcement learning have also proposed to disentangle representation of both states (Engel & Mannor, 2001; Littman & Sutton, 2002; Stooke et al., 2020; Zhu et al., 2020), and actions (Tennenholtz & Mannor, 2019; Chandak et al., 2019). These allow for the abstraction of states and actions to significantly decrease computation requirements, by e.g., decreasing the effective dimensionality of the action space (Tennenholtz & Mannor, 2019). Unlike previous work, GELATO is focused on measuring proximity and uncertainty for the purpose of mitigating the OOD problem and enhancing offline reinforcement learning performance.

## 8. Negative Results and Future Work

This work presented GELATO, an offline RL framework with strong flexibility and robustness for OOD detection. While our method showed an increase in performance, various improvements could still be applied.

First, we note that our method was significantly slower – comparably, 5 times slower than using the decoder’s variance for uncertainty estimation. The apparent slowdown in performance was mostly due to computation of the geodesic distance. Improvement in this area may utilize techniques for efficient geodesic estimation (Chen et al., 2018; 2019).

Second, using neural networks to estimate the variance  $\sigma$  may generally result in a poor measure of uncertainty, due to uncontrolled extrapolations of the neural network to arbitrary regions of the latent space, i.e., areas of little data. More involved methods for uncertainty estimation of variational models, including RBF networks (Arvanitidis et al., 2018) and Likelihood Regret (Xiao et al., 2020) can be used to improve the uncertainty element of our proposed metric.

We conclude by noting possible future applications of our work. In Section 6.1 we demonstrated the inherent geometry our model had captured, its corresponding metric, and geodesics. Still, in this work we focused specifically on metrics related to the decoded state. In fact, a similar derivation to Proposition 2 could be applied to other modeled statistics, e.g., Q-values, rewards, future actions, and more. Each distinct statistic would induce its own unique metric w.r.t. its respective probability measure. Particularly, this concept may benefit a vast array of applications in continuous or large state and action spaces, with adaptability w.r.t. proximity and uncertainty as part of a newly proposed metric.

## References

- Agarwal, R., Schuurmans, D., and Norouzi, M. An optimistic perspective on offline reinforcement learning. In *International Conference on Machine Learning*, pp. 104–114. PMLR, 2020.
- Arvanitidis, G., Hansen, L. K., and Hauberg, S. Maximum likelihood estimation of riemannian metrics from euclidean data. In *International Conference on Geometric Science of Information*, pp. 38–46. Springer, 2017.
- Arvanitidis, G., Hansen, L. K., and Hauberg, S. Latent space oddity: On the curvature of deep generative models. In *6th International Conference on Learning Representations, ICLR 2018*, 2018.
- Arvanitidis, G., Hauberg, S., and Schölkopf, B. Geometrically enriched latent spaces. *arXiv preprint arXiv:2008.00565*, 2020.
- Bojanowski, P., Joulin, A., Lopez-Pas, D., and Szlam, A. Optimizing the latent space of generative networks. In *International Conference on Machine Learning*, pp. 600–609, 2018.
- Buckman, J., Gelada, C., and Bellemare, M. G. The importance of pessimism in fixed-dataset policy optimization. *arXiv preprint arXiv:2009.06799*, 2020.
- Carmo, M. P. d. *Riemannian geometry*. Birkhäuser, 1992.
- Chandak, Y., Theodorou, G., Kostas, J., Jordan, S., and Thomas, P. Learning action representations for reinforcement learning. In *International Conference on Machine Learning*, pp. 941–950, 2019.
- Chen, N., Klushyn, A., Kurle, R., Jiang, X., Bayer, J., and Smagt, P. Metrics for deep generative models. In *International Conference on Artificial Intelligence and Statistics*, pp. 1540–1550. PMLR, 2018.
- Chen, N., Ferroni, F., Klushyn, A., Paraschos, A., Bayer, J., and van der Smagt, P. Fast approximate geodesics for deep generative models. In *International Conference on Artificial Neural Networks*, pp. 554–566. Springer, 2019.
- Chen, N., Klushyn, A., Ferroni, F., Bayer, J., and van der Smagt, P. Learning flat latent manifolds with vaes. 2020a.
- Chen, X., Kingma, D. P., Salimans, T., Duan, Y., Dhariwal, P., Schulman, J., Sutskever, I., and Abbeel, P. Variational lossy autoencoder. *arXiv preprint arXiv:1611.02731*, 2016.
- Chen, X., Zhou, Z., Wang, Z., Wang, C., Wu, Y., and Ross, K. Bail: Best-action imitation learning for batch deep reinforcement learning. *Advances in Neural Information Processing Systems*, 33, 2020b.
- Ding, Z., Xu, Y., Xu, W., Parmar, G., Yang, Y., Welling, M., and Tu, Z. Guided variational autoencoder for disentanglement learning. In *Proceedings of the IEEE/CVF Conference on Computer Vision and Pattern Recognition*, pp. 7920–7929, 2020.
- Dinh, L., Krueger, D., and Bengio, Y. Nice: Non-linear independent components estimation. *arXiv preprint arXiv:1410.8516*, 2014.
- Engel, J., Hoffman, M., and Roberts, A. Latent constraints: Learning to generate conditionally from unconditional generative models. *arXiv preprint arXiv:1711.05772*, 2017.
- Engel, Y. and Mannor, S. Learning embedded maps of markov processes. In *Proceedings of the Eighteenth International Conference on Machine Learning*, pp. 138–145, 2001.
- Ernst, D., Geurts, P., and Wehenkel, L. Tree-based batch mode reinforcement learning. *Journal of Machine Learning Research*, 6(Apr):503–556, 2005.
- Fedus, W., Ramachandran, P., Agarwal, R., Bengio, Y., Larochelle, H., Rowland, M., and Dabney, W. Revisiting fundamentals of experience replay. In *International Conference on Machine Learning*, pp. 3061–3071. PMLR, 2020.
- Fonteneau, R., Murphy, S. A., Wehenkel, L., and Ernst, D. Batch mode reinforcement learning based on the synthesis of artificial trajectories. *Annals of operations research*, 208(1):383–416, 2013.
- Fu, J., Kumar, A., Soh, M., and Levine, S. Diagnosing bottlenecks in deep q-learning algorithms. In *International Conference on Machine Learning*, pp. 2021–2030, 2019.
- Fu, J., Kumar, A., Nachum, O., Tucker, G., and Levine, S. D4rl: Datasets for deep data-driven reinforcement learning. *arXiv preprint arXiv:2004.07219*, 2020.
- Fujimoto, S., Meger, D., and Precup, D. Off-policy deep reinforcement learning without exploration. In *International Conference on Machine Learning*, pp. 2052–2062. PMLR, 2019.
- Gal, Y. and Ghahramani, Z. Dropout as a bayesian approximation: Representing model uncertainty in deep learning. In *international conference on machine learning*, pp. 1050–1059, 2016.
- Goodfellow, I., Bengio, Y., Courville, A., and Bengio, Y. *Deep learning*, volume 1. MIT press Cambridge, 2016.
- Guss, W. H., Houghton, B., Topin, N., Wang, P., Codel, C., Veloso, M., and Salakhutdinov, R. MineRL: A large-scale dataset of Minecraft demonstrations. *Twenty-Eighth*

- International Joint Conference on Artificial Intelligence*, 2019. URL <http://miner1.io>.
- Haarnoja, T., Zhou, A., Abbeel, P., and Levine, S. Soft actor-critic: Off-policy maximum entropy deep reinforcement learning with a stochastic actor. In *International Conference on Machine Learning*, pp. 1861–1870. PMLR, 2018.
- Hafner, D., Lillicrap, T., Ba, J., and Norouzi, M. Dream to control: Learning behaviors by latent imagination. In *International Conference on Learning Representations*, 2019.
- Hafner, D., Lillicrap, T., Norouzi, M., and Ba, J. Mastering atari with discrete world models. *arXiv preprint arXiv:2010.02193*, 2020.
- Hausman, K., Springenberg, J. T., Wang, Z., Heess, N., and Riedmiller, M. Learning an embedding space for transferable robot skills. In *International Conference on Learning Representations*, 2018.
- Hsu, W.-N., Zhang, Y., and Glass, J. Unsupervised learning of disentangled and interpretable representations from sequential data. In *Advances in neural information processing systems*, pp. 1878–1889, 2017.
- Jaksch, T., Ortner, R., and Auer, P. Near-optimal regret bounds for reinforcement learning. *Journal of Machine Learning Research*, 11(4), 2010.
- Janner, M., Fu, J., Zhang, M., and Levine, S. When to trust your model: Model-based policy optimization. *arXiv preprint arXiv:1906.08253*, 2019.
- Johnson, J., Douze, M., and Jégou, H. Billion-scale similarity search with gpus. *IEEE Transactions on Big Data*, 2019.
- Kalatzis, D., Eklund, D., Arvanitidis, G., and Hauberg, S. Variational autoencoders with riemannian brownian motion priors. In *Proceedings of the 37th International Conference on Machine Learning (ICML)*. PMLR, 2020.
- Kidambi, R., Rajeswaran, A., Netrapalli, P., and Joachims, T. Morel: Model-based offline reinforcement learning. *arXiv preprint arXiv:2005.05951*, 2020.
- Kingma, D. P. and Ba, J. Adam: A method for stochastic optimization. *arXiv preprint arXiv:1412.6980*, 2014.
- Kingma, D. P. and Welling, M. Auto-encoding variational bayes. *arXiv preprint arXiv:1312.6114*, 2013.
- Kingma, D. P., Mohamed, S., Jimenez Rezende, D., and Welling, M. Semi-supervised learning with deep generative models. *Advances in neural information processing systems*, 27:3581–3589, 2014.
- Klushyn, A., Chen, N., Kurle, R., Cseke, B., and van der Smagt, P. Learning hierarchical priors in vaes. In *Advances in Neural Information Processing Systems*, pp. 2870–2879, 2019.
- Kumar, A., Fu, J., Soh, M., Tucker, G., and Levine, S. Stabilizing off-policy q-learning via bootstrapping error reduction. In *Advances in Neural Information Processing Systems*, pp. 11784–11794, 2019.
- Kumar, A., Zhou, A., Tucker, G., and Levine, S. Conservative q-learning for offline reinforcement learning. *arXiv preprint arXiv:2006.04779*, 2020.
- Lakshminarayanan, B., Pritzel, A., and Blundell, C. Simple and scalable predictive uncertainty estimation using deep ensembles. In *Advances in neural information processing systems*, pp. 6402–6413, 2017.
- Laroche, R., Trichelair, P., and Des Combes, R. T. Safe policy improvement with baseline bootstrapping. In *International Conference on Machine Learning*, pp. 3652–3661. PMLR, 2019.
- Levine, S., Kumar, A., Tucker, G., and Fu, J. Offline reinforcement learning: Tutorial, review, and perspectives on open problems. *arXiv preprint arXiv:2005.01643*, 2020.
- Li, M., Wu, L., Jun, W., and Ammar, H. B. Multi-view reinforcement learning. In *Advances in neural information processing systems*, pp. 1420–1431, 2019.
- Littman, M. L. and Sutton, R. S. Predictive representations of state. In *Advances in neural information processing systems*, pp. 1555–1561, 2002.
- Nalisnick, E., Matsukawa, A., Teh, Y. W., Gorur, D., and Lakshminarayanan, B. Do deep generative models know what they don’t know? *arXiv preprint arXiv:1810.09136*, 2018.
- Osband, I., Blundell, C., Pritzel, A., and Van Roy, B. Deep exploration via bootstrapped dqn. In *Advances in neural information processing systems*, pp. 4026–4034, 2016.
- O’Donoghue, B., Osband, I., Munos, R., and Mnih, V. The uncertainty bellman equation and exploration. In *International Conference on Machine Learning*, pp. 3836–3845, 2018.
- Petangoda, J. C., Pascual-Diaz, S., Adam, V., Vrancx, P., and Grau-Moya, J. Disentangled skill embeddings for reinforcement learning. *arXiv preprint arXiv:1906.09223*, 2019.
- Ren, J., Liu, P. J., Fertig, E., Snoek, J., Poplin, R., Deprieto, M., Dillon, J., and Lakshminarayanan, B. Likelihood ratios for out-of-distribution detection. In *Advances in Neural Information Processing Systems*, pp. 14707–14718, 2019.

- Rezende, D. J., Mohamed, S., and Wierstra, D. Stochastic backpropagation and approximate inference in deep generative models. *arXiv preprint arXiv:1401.4082*, 2014.
- Riedmiller, M. Neural fitted q iteration—first experiences with a data efficient neural reinforcement learning method. In *European Conference on Machine Learning*, pp. 317–328. Springer, 2005.
- Rybkin, O., Daniilidis, K., and Levine, S. Simple and effective vae training with calibrated decoders. *arXiv preprint arXiv:2006.13202*, 2020.
- Schaal, S. Is imitation learning the route to humanoid robots? *Trends in cognitive sciences*, 3(6):233–242, 1999.
- Senge, R., Bösner, S., Dembczyński, K., Haasenritter, J., Hirsch, O., Donner-Banzhoff, N., and Hüllermeier, E. Reliable classification: Learning classifiers that distinguish aleatoric and epistemic uncertainty. *Information Sciences*, 255:16–29, 2014.
- Serban, I., Sordoni, A., Lowe, R., Charlin, L., Pineau, J., Courville, A., and Bengio, Y. A hierarchical latent variable encoder-decoder model for generating dialogues. In *Proceedings of the AAAI Conference on Artificial Intelligence*, volume 31, 2017.
- Sønderby, C. K., Raiko, T., Maaløe, L., Sønderby, S. K., and Winther, O. Ladder variational autoencoders. In *Advances in neural information processing systems*, pp. 3738–3746, 2016.
- Stooke, A., Lee, K., Abbeel, P., and Laskin, M. Decoupling representation learning from reinforcement learning. *arXiv preprint arXiv:2009.08319*, 2020.
- Sutton, R. S., Barto, A. G., et al. *Introduction to reinforcement learning*, volume 135. MIT press Cambridge, 1998.
- Swazinna, P., Udluft, S., and Runkler, T. Overcoming model bias for robust offline deep reinforcement learning. *arXiv preprint arXiv:2008.05533*, 2020.
- Tennenholtz, G. and Mannor, S. The natural language of actions. In *International Conference on Machine Learning*, pp. 6196–6205, 2019.
- Todorov, E., Erez, T., and Tassa, Y. Mujoco: A physics engine for model-based control. In *2012 IEEE/RSJ International Conference on Intelligent Robots and Systems*, pp. 5026–5033. IEEE, 2012.
- Vahdat, A. and Kautz, J. Nvae: A deep hierarchical variational autoencoder. *arXiv preprint arXiv:2007.03898*, 2020.
- Van Den Oord, A., Vinyals, O., et al. Neural discrete representation learning. In *Advances in Neural Information Processing Systems*, pp. 6306–6315, 2017.
- Wang, R., Foster, D. P., and Kakade, S. M. What are the statistical limits of offline rl with linear function approximation? *arXiv preprint arXiv:2010.11895*, 2020.
- Xiao, Z., Yan, Q., and Amit, Y. Likelihood regret: An out-of-distribution detection score for variational auto-encoder. *Advances in Neural Information Processing Systems*, 33, 2020.
- Yu, T., Thomas, G., Yu, L., Ermon, S., Zou, J., Levine, S., Finn, C., and Ma, T. Mopo: Model-based offline policy optimization. *arXiv preprint arXiv:2005.13239*, 2020.
- Zanette, A. Exponential lower bounds for batch reinforcement learning: Batch rl can be exponentially harder than online rl. *arXiv preprint arXiv:2012.08005*, 2020.
- Zhu, J., Xia, Y., Wu, L., Deng, J., Zhou, W., Qin, T., and Li, H. Masked contrastive representation learning for reinforcement learning. *arXiv preprint arXiv:2010.07470*, 2020.

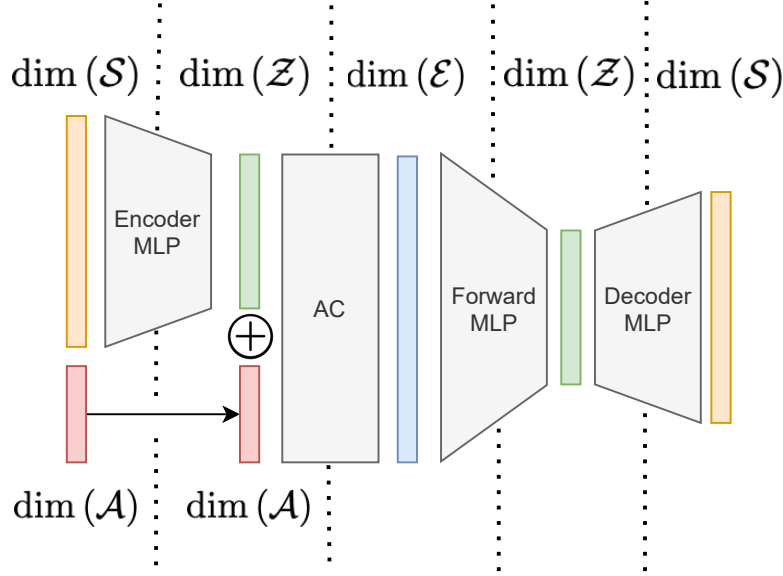


Figure 5. Latent model architecture (does not depict reward MLP).

## Appendix

### 9. Specific Implementation Details

#### 9.1. Variational Model

As a preprocessing step rewards were normalized to values between  $[-1, 1]$ . We trained our variational model with latent dimensions  $\dim(\mathcal{Z}) = 32$  and  $\dim(\mathcal{E}) = \dim(\mathcal{Z}) + \dim(\mathcal{A})$ . All domains were trained with the same hyperparameters. Specifically, we used a 2-layer Multi Layer Perceptron (MLP) to encode  $\mathcal{Z}$ , after which a 2-layer Affine Coupling (AC) (Dinh et al., 2014) was used to encode  $\mathcal{E}$ . We also used a 2-layer MLP for the forward, reward, and decoder models. All layers contained 256 hidden layers.

The latent model was trained in two separate phases for 100k and 50k steps each by stochastic gradient descent and the ADAM optimizer (Kingma & Ba, 2014). First, the model was fully trained using a calibrated Gaussian decoder (Rybkin et al., 2020). Specifically, a maximum-likelihood estimate of the variance was used  $\sigma^* = \text{MSE}(\mu, \hat{\mu}) \in \arg \max_{\sigma} \mathcal{N}(\hat{\mu} | \mu, \sigma^2 I)$ . Finally, in the second stage we fit the variance decoder network. We found this process of to greatly improve convergence speed and accuracy, and mitigate posterior collapse. We used a minimum variance of 0.01 for all of our stochastic models.

To further stabilize training we used a momentum encoder. Specifically we updated a target encoder as a slowly moving average of the weights from the learned encoder as

$$\bar{\theta} \leftarrow (1 - \tau)\bar{\theta} + \tau\theta$$

Hyperparameters for our variational model are summarized in Table 2. The latent architecture is visualized in Figure 5.

Parameter	Value	Parameter	Value
$\dim(\mathcal{Z})$	32	LEARNING RATE	$10^{-3}$
$\dim(\mathcal{E})$	$32 + \dim(\mathcal{A})$	BATCH SIZE	128
ENCODER MLP HIDDEN	256, 256	TARGET UPDATE $\tau$	0.01
FORWARD MLP HIDDEN	256, 256	TARGET UPDATE INTERVAL	1
DECODER MLP HIDDEN	256, 256	PHASE 1 UPDATES	100000
REWARD MLP HIDDEN	256, 256	PHASE 2 UPDATES	50000

Table 2. Hyper parameters for variational model

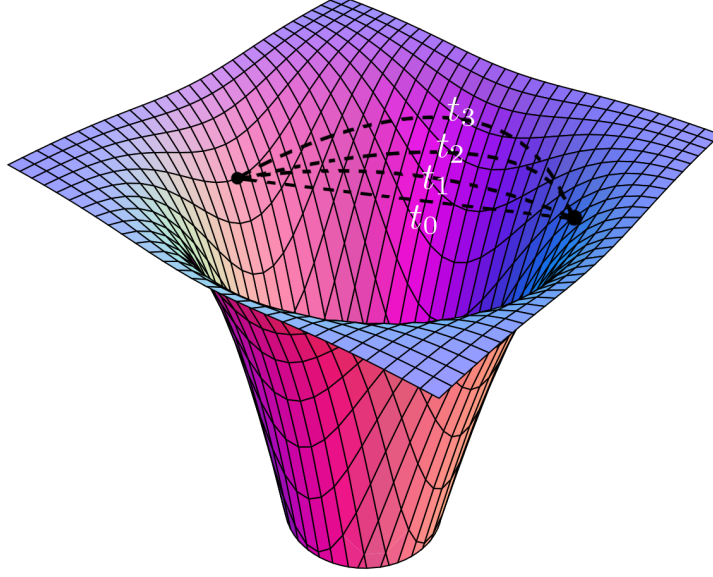


Figure 6. Illustration of geodesic curve optimization in Algorithm 2.

---

**Algorithm 2** Geodesic Distance Estimation
 

---

**Input:** forward latent  $F$ , decoder  $D$ , learning rate  $\lambda$ , number of iterations  $T$ , grid size  $n$ , eval points  $e_0, e_1$

**Initialize:** parametric curve  $\gamma_\theta : \gamma_\theta(0) = e_0, \gamma_\theta(1) = e_1$

**for**  $t = 1$  **to**  $T$  **do**

$$L_\mu(\theta) \leftarrow \sum_{i=1}^n \mu_D(\mu_F(\gamma_\theta(\frac{i}{n}))) - \mu_D(\mu_F(\gamma_\theta(\frac{i-1}{n})))$$

$$L_\sigma(\theta) \leftarrow \sum_{i=1}^n \sigma_D(\mu_F(\gamma_\theta(\frac{i}{n}))) - \sigma_D(\mu_F(\gamma_\theta(\frac{i-1}{n})))$$

$$L(\theta) \leftarrow L_\mu(\theta) + L_\sigma(\theta)$$

$$\theta \leftarrow \theta - \lambda \nabla_\theta L(\theta)$$

**end for**

$$G_{D \circ F} = J_{\mu_F}^T \overline{G}_D J_{\mu_F} + J_{\sigma_F}^T \text{diag}(\overline{G}_D) J_{\sigma_F}$$

$$\forall i, \Delta_i \leftarrow \gamma_\theta(\frac{i}{n}) - \gamma_\theta(\frac{i-1}{n})$$

$$d(e_0, e_1) \leftarrow \sum_{i=1}^n \left( \frac{\partial \gamma_\theta}{\partial t} \Big|_{\frac{i}{n}} \right)^T G_{D \circ F}(\gamma_\theta(\frac{i}{n})) \left( \frac{\partial \gamma_\theta}{\partial t} \Big|_{\frac{i}{n}} \right) \Delta_i$$

**Return:**  $d(e_0, e_1)$

---

## 9.2. Geodesic Distance Estimation

In order to practically estimate the geodesic distance between two points  $e_1, e_2 \in \mathcal{E}$  we defined a parametric curve in latent space and used gradient descent to minimize the curve’s energy <sup>2</sup>. The resulting curve and pullback metric were then used to calculate the geodesic distance by a numerical estimate of the curve length (Equation (7)).

Pseudo code for Geodesic Distance Estimation is shown in Algorithm 2. Our curve was modeled as a cubic spline with 8 coefficients. We used SGD (momentum 0.99) to optimize the curve energy over 20 gradient iterations with a grid of 10 points and a learning rate of  $10^{-3}$ . An illustration of the convergence of such a curve is illustrated in Figure 6

## 9.3. RL algorithm

Our learning algorithm is based on the Soft Learning framework proposed in Algorithm 2 of Yu et al. (2020). Pseudo code is shown in Algorithm 3. Specifically we used two replay buffers  $\mathcal{R}_{\text{model}}, \mathcal{R}_{\text{data}}$ , where  $|\mathcal{R}_{\text{model}}| = 50000$  and  $\mathcal{R}_{\text{data}}$  contained the full offline dataset. In every epoch an initial state  $s_0$  was sampled from the offline dataset and embedded using our latent

<sup>2</sup>Other methods for computing the geodesic distance include solving a system of ODEs (Arvanitidis et al., 2018), using graph based geodesics (Chen et al., 2019), or using neural networks (Chen et al., 2018).

**Algorithm 3** GELATO with Soft Learning

---

**Input:** Reward penalty coefficient  $\lambda$ , rollout horizon  $h$ , rollout batch size  $b$ , training epochs  $T$ , number of neighbors  $K$ .  
 Train variational latent forward model on dataset  $\mathcal{D}$  by maximizing ELBO (Equation (5))  
 Construct embedded dataset  $\mathcal{D}_{\text{embd}} = \{E_i\}_{i=1}^n$  using latent model to initialize KNN.  
 Initialize policy  $\pi$  and empty replay buffer  $\mathcal{R}_{\text{model}} \leftarrow \emptyset$ .  
**for** epoch = 1 **to**  $T$  **do**  
     **for**  $i = 1$  **to**  $b$  (in parallel) **do**  
         Sample state  $s_1$  from  $\mathcal{D}$  for the initialization of the rollout and embed using latent model to produce  $z_1$ .  
         **for**  $j = 1$  **to**  $h$  **do**  
             Sample an action  $a_j \sim \pi(\cdot|z_j)$ .  
             Embed  $(z_j, a_j) \rightarrow E_{z_j, a_j}$  using latent model  
             Sample  $z_{j+1}$  from latent forward model  $F(E_{z_j, a_j})$ .  
             Sample  $r_j$  from latent reward model  $R(E_{z_j, a_j})$ .  
             Use Algorithm 2 to compute  $K$  nearest neighbors  $\{\text{NN}_{z_j, a_j}^{(k)}\}_{k=1}^K$  and their distances  $\{d_k\}_{k=1}^N$  to  $E_{z_j, a_j}$ .  
             Compute  $\tilde{r}_j = r_j - \lambda \left( \frac{1}{K} \sum_{k=1}^K d_k \right)$   
             Add sample  $(z_j, a_j, \tilde{r}_j, z_{j+1})$  to  $\mathcal{R}_{\text{model}}$ .  
         **end for**  
     **end for**  
     Drawing samples from  $\mathcal{R}_{\text{data}} \cup \mathcal{R}_{\text{model}}$ , use SAC to update  $\pi$ .  
**end for**

---

model to generate  $z_0 \in \mathcal{Z}$ . During rollouts of  $\pi$ , embeddings  $E_{z,a} \in \mathcal{E}$  were then generated from  $z$  and used to (1) sample next latent state  $z'$ , (2) sample estimated rewards  $r$ , and (3) compute distances to  $K = 20$  nearest neighbors in embedded the dataset.

We used Algorithm 2 to compute the geodesic distances, and FAISS (Johnson et al., 2019) for efficient nearest neighbor computation on GPUs. To stabilize learning, we normalized the penalty  $\frac{1}{K} \sum_{k=1}^K d_k$  according to the maximum penalty, ensuring penalty lies in  $[0, 1]$  (recall that the latent reward predictor was trained over normalized rewards in  $[-1, 1]$ ). For the non-skewed version of GELATO, we used  $\lambda = 1$  as our reward penalty coefficient and  $\lambda = 2$  for the skewed versions. We used rollout horizon of  $h = 5$ , and did not notice significant performance improvement for different values of  $h$ .

## 10. Uncertainty Estimation Methods

Using neural networks to estimate the variance  $\sigma(z)$  may result in a poor measure of uncertainty, due to uncontrolled extrapolations of the neural network to arbitrary regions of the latent space, i.e., areas of little data. One method to overcome this is using an ensemble of models or decoder networks. Nevertheless, this approach is computationally expensive, and thus not a favorable solution for large or complex models.

Instead, Arvanitidis et al. (2017) showed that modeling the inverse variance  $\beta(z) = (\sigma^2(z))^{-1}$  with a positive Radial Basis Function (RBF) network achieves a reliable uncertainty estimate, with well-behaved extrapolations in latent space, as it requires high variance in regions that are far from the data. Formally the RBF network is defined as follows. We denote  $\sigma(z) = \sqrt{(\beta(z))^{-1}}$  where

$$\begin{aligned} \beta(z) &= W^T \phi(z), \\ \phi_i(z) &= \exp\left(-\frac{1}{2} \lambda_i \|z - c_i\|_2^2\right), \end{aligned}$$

$W$  are the positive learned weights of the network,  $\lambda_i$  the bandwidth, and  $c_i$  the centers trained using  $k$ -means over the learned latent representations of the offline data.

We tested GELATO on D4RL Mujoco benchmarks (see Section 6) with RBF networks. Specifically, we followed a similar training procedure with two training phases. In the first training phase we trained our variational model with a calibrated decoder as before. In the second training phase we used  $k$ -means to cluster our dataset to 128 clusters, after which an RBF network was trained for a second phase of 50000 iterations.

	Hopper		
Method	Random	Medium	Med-Expert
GELATO	685 $\pm$ 15	1676 $\pm$ 223	574 $\pm$ 16
GELATO-RBF	613 $\pm$ 24	1700 $\pm$ 319	498 $\pm$ 55

Table 3. Performance of GELATO with RBF decoder.

Results for GELATO with RBF decoder networks for the Hopper environment are presented in Table 3. We did not find significant improvement in using RBF networks over decoder variance. We believe this is due to the smoothness in ambient space, allowing for well behaved extrapolations of uncertainty. We conjecture RBF networks may show improved performance on higher dimensional problems (e.g., images), yet we leave this for future work, as these may involve utilizing more involved state-of-the-art variational models (Vahdat & Kautz, 2020).

## 11. Derivation of Variational Lower Bound

Recall our graphical model from Section 4

$$P(s_0, a_0, r_0, \dots, s_h, a_h, r_h) = \int_{z_0, \dots, z_h} P(z_0) \prod_{i=0}^h P(s_i | z_i) \pi(a_i | s_i) P(r_i | E_{z_i, a_i}) \prod_{j=1}^h P(z_j | E_{z_{j-1}, a_{j-1}}) dz_0 \dots dz_h.$$

To clear notations we define  $E_{z_{-1}, a_{-1}} = 0$ , so that we can rewrite the above expression as

$$P(s_0, a_0, r_0, \dots, s_h, a_h, r_h) = \int_{z_0, \dots, z_h} \prod_{i=0}^h P(s_i | z_i) \pi(a_i | s_i) P(r_i | E_{z_i, a_i}) P(z_j | E_{z_{-1}, a_{-1}})$$

Introducing  $q(z_i | s_i)$  we can write

$$\begin{aligned} & \log \int_{z_0, \dots, z_h} \prod_{i=0}^h \frac{q(z_i | s_i)}{q(z_i | s_i)} \prod_{i=0}^h P(s_i | z_i) \pi(a_i | s_i) P(r_i | E_{z_i, a_i}) P(z_j | E_{z_{-1}, a_{-1}}) \\ & \geq \int_{z_0, \dots, z_h} \prod_{i=0}^h q(z_i | s_i) \left( \sum_{i=0}^h \log \left( \frac{P(s_i | z_i) \pi(a_i | s_i) P(r_i | E_{z_i, a_i}) P(z_j | E_{z_{-1}, a_{-1}})}{q(z_i | s_i)} \right) \right) \\ & = \sum_{i=0}^H \mathbb{E}_{q(z_i | s_i)} \left[ \log(P(s_i | z_i) \pi(a_i | s_i) P(r_i | E_{z_i, a_i})) \right] \\ & \quad - \sum_{i=0}^{H-1} \mathbb{E}_{q(z_i | s_i)} \left[ D_{KL}(q(z_{i+1} | s_{i+1}) || P(z_{i+1} | E_{z_i, a_i})) \right] \\ & \quad - D_{KL}(q(z_0 | s_0) || P(z_0)). \end{aligned}$$

## 12. Proof of Proposition 2

**Proposition 2.** Let  $F : \mathcal{E} \mapsto \mathcal{Z}$ , and  $D : \mathcal{Z} \mapsto \mathcal{S}$  as defined above. Then, the expected pullback metric of the composite function  $(D \circ F) : \mathcal{E} \mapsto \mathcal{S}$  is given by

$$\mathbb{E}[G_{D \circ F}] = J_{\mu_F}^T \overline{G}_D J_{\mu_F} + J_{\sigma_F}^T \text{diag}(\overline{G}_D) J_{\sigma_F},$$

where here,  $\overline{G}_D = \mathbb{E}_{z' \sim F} [J_{\mu_D}^T J_{\mu_D} + J_{\sigma_D}^T J_{\sigma_D}]$  is the expected pullback metric of  $D$ .

*Proof.* We can write  $z' = \mu_F(z) + \sigma_F(z) \odot \epsilon_F$  and  $s' = \mu_D(z') + \sigma_D(z') \odot \epsilon_D$  where  $\epsilon_F \sim \mathcal{N}(0, I_d)$ ,  $\epsilon_D \sim \mathcal{N}(0, I_K)$ ,  $\mu_F : \mathbb{R}^d \mapsto \mathbb{R}^\ell$ ,  $\mu_D : \mathbb{R}^\ell \mapsto \mathbb{R}^K$  and  $\sigma_F : \mathbb{R}^d \mapsto \mathbb{R}^\ell$ ,  $\sigma_D : \mathbb{R}^\ell \mapsto \mathbb{R}^K$ .

Applying the chain rule we get

$$J_{D \circ F} = \frac{\partial(D \circ F)}{\partial z} = J_{\mu_D} J_{\mu_F} + J_{\mu_D} B_{\epsilon_F} + B_{\epsilon_D} J_{\mu_F} + B_{\epsilon_D} B_{\epsilon_F}$$

where

$$\begin{aligned} B_{\epsilon_F} &= (S_{F,1\epsilon_F}, S_{F,2\epsilon_F}, \dots, S_{F,d\epsilon_F})_{d \times d}, \\ S_{F,i} &= \text{diag}\left(\frac{\partial \sigma_F^1}{\partial z_i}, \frac{\partial \sigma_F^2}{\partial z_i}, \dots, \frac{\partial \sigma_F^d}{\partial z_i}\right)_{d \times d}, \quad \text{and} \\ B_{\epsilon_D} &= (S_{D,1\epsilon_D}, S_{D,2\epsilon_D}, \dots, S_{D,d\epsilon_D})_{K \times d}, \\ S_{D,i} &= \text{diag}\left(\frac{\partial \sigma_D^1}{\partial z'_i}, \frac{\partial \sigma_D^2}{\partial z'_i}, \dots, \frac{\partial \sigma_D^d}{\partial z'_i}\right)_{K \times K}. \end{aligned}$$

This yields

$$\begin{aligned} \mathbb{E}[J_{F \circ D}^T J_{F \circ D}] &= \mathbb{E}\left[(J_{\mu_D} J_{\mu_F} + J_{\mu_D} B_{\epsilon_F} + B_{\epsilon_D} J_{\mu_F} + B_{\epsilon_D} B_{\epsilon_F})^T (J_{\mu_D} J_{\mu_F} + J_{\mu_D} B_{\epsilon_F} + B_{\epsilon_D} J_{\mu_F} + B_{\epsilon_D} B_{\epsilon_F})\right] \\ &= J_{\mu_F}^T J_{\mu_D}^T J_{\mu_D} J_{\mu_F} + \mathbb{E}[B_{\epsilon_F}^T J_{\mu_D}^T J_{\mu_D} B_{\epsilon_F}] + \mathbb{E}[J_{\mu_F}^T B_{\epsilon_D}^T B_{\epsilon_D} J_{\mu_F}] + \mathbb{E}[B_{\epsilon_F}^T B_{\epsilon_D}^T B_{\epsilon_D} B_{\epsilon_F}] \\ &= J_{\mu_F}^T (J_{\mu_D}^T J_{\mu_D} + \mathbb{E}[B_{\epsilon_D}^T B_{\epsilon_D}]) J_{\mu_F} + \mathbb{E}[B_{\epsilon_F}^T (J_{\mu_D}^T J_{\mu_D} + B_{\epsilon_D}^T B_{\epsilon_D}) B_{\epsilon_F}] \end{aligned}$$

where in the second equality we used the fact that  $\epsilon_D, \epsilon_F$  are independent and  $\mathbb{E}[B_\epsilon] = 0$ . By Lemma 1 we have

$$\mathbb{E}[B_{\epsilon_D}^T B_{\epsilon_D}] = J_{\sigma_D}^T J_{\sigma_D}.$$

Similarly,

$$\mathbb{E}[B_{\epsilon_F}^T B_{\epsilon_D}^T B_{\epsilon_D} B_{\epsilon_F}] = \mathbb{E}[\mathbb{E}[B_{\epsilon_F}^T B_{\epsilon_D}^T B_{\epsilon_D} B_{\epsilon_F} | \epsilon_F]] = \mathbb{E}[B_{\epsilon_F}^T J_{\sigma_D}^T J_{\sigma_D} B_{\epsilon_F}] = J_{\sigma_F}^T \text{diag}(J_{\sigma_F}^T J_{\sigma_F}) J_{\sigma_F}$$

Finally,

$$\mathbb{E}[B_{\epsilon_F}^T J_{\mu_D}^T J_{\mu_D} B_{\epsilon_F}] = J_{\sigma_F}^T \text{diag}(J_{\mu_D}^T J_{\mu_D}) J_{\sigma_F}.$$

This completes the proof.  $\square$

**Lemma 1.** Let  $\epsilon \sim \mathcal{N}(0, I_K)$ ,  $f : \mathbb{R}^d \mapsto \mathbb{R}^K$ ,  $A \in \mathbb{R}^{K \times K}$ . Denote  $S_i = \text{diag}\left(\frac{\partial f^1}{\partial z_i}, \frac{\partial f^2}{\partial z_i}, \dots, \frac{\partial f^K}{\partial z_i}\right)$  for  $1 \leq i \leq d$  and

$$B = [S_1 \epsilon, S_2 \epsilon, \dots, S_d \epsilon]_{K \times d}.$$

Then  $\mathbb{E}[B^T A B] = J_f^T \text{diag}(A) J_f$ .

*Proof.* We have that

$$\begin{aligned} \mathbb{E}[B^T A B] &= \mathbb{E}\left[\begin{bmatrix} \epsilon^T S_1^T \\ \epsilon^T S_2^T \\ \vdots \\ \epsilon^T S_d^T \end{bmatrix} A [S_1 \epsilon, S_2 \epsilon, \dots, S_d \epsilon]\right] \\ &= \begin{bmatrix} \mathbb{E}[\epsilon^T S_1^T A S_1 \epsilon], \mathbb{E}[\epsilon^T S_1^T A S_2 \epsilon], \dots, \mathbb{E}[\epsilon^T S_1^T A S_d \epsilon], \\ \mathbb{E}[\epsilon^T S_2^T A S_1 \epsilon], \mathbb{E}[\epsilon^T S_2^T A S_2 \epsilon], \dots, \mathbb{E}[\epsilon^T S_2^T A S_d \epsilon], \\ \vdots \\ \mathbb{E}[\epsilon^T S_d^T A S_1 \epsilon], \mathbb{E}[\epsilon^T S_d^T A S_2 \epsilon], \dots, \mathbb{E}[\epsilon^T S_d^T A S_d \epsilon] \end{bmatrix}. \end{aligned}$$

Finally notice that for any matrix  $M$

$$\mathbb{E}[\epsilon^T M \epsilon] = \sum_{i=1}^d \sum_{j=1}^d M_{ij} \mathbb{E}[\epsilon_i \epsilon_j] = \sum_{i=1}^d M_{ii} = \text{trace}(M).$$

Then,

$$\mathbb{E} [B^T AB] = \begin{bmatrix} \text{trace}(S_1^T AS_1), \text{trace}(S_1^T AS_2), \dots, \text{trace}(S_1^T AS_d) \\ \text{trace}(S_2^T AS_1), \text{trace}(S_2^T AS_2), \dots, \text{trace}(S_2^T AS_d) \\ \vdots \\ \text{trace}(S_d^T AS_1), \text{trace}(S_d^T AS_2), \dots, \text{trace}(S_d^T AS_d) \end{bmatrix}.$$

□

Next, note that

$$\text{trace}(S_i AS_j) = \sum_{k=1}^K \frac{\partial f^k}{\partial z_i} \frac{\partial f^k}{\partial z_j} A_{kk}.$$

Therefore,

$$\mathbb{E} [B^T AB] = J_f^T \text{diag}(A) J_f.$$